Contents lists available at ScienceDirect

Physics Letters A

Internal energy exchanges and chaotic dynamics in an intrinsically coupled system

M. C. de Sousa [a,b], A.B. Schelin [c], F.A. Marcus [a], R. L. Viana [d,a], I. L. Caldas [a]

[a] *Instituto de Fisica, Universidade de Sao Paulo, 05508-090 Sao Paulo, Brazil*
[b] *LSI, CEA/DRF/IRAMIS, CNRS, Ecole Polytechnique, Institut Polytechnique de Paris, F-91128 Palaiseau, France*
[c] *Instituto de Fisica, Universidade de Brasilia, 70919-970 Brasilia, Brazil*
[d] *Departamento de Fisica, Universidade Federal do Parana, 81531-980 Curitiba, Brazil*

ARTICLE INFO

ABSTRACT

Intrinsically coupled nonlinear systems typically present different oscillating components that exchange energy among themselves. A paradigmatic example is the spring pendulum, for which we identify spring, pendulum, and coupled oscillations. We propose a new approach that properly accounts for the nonlinear coupling, and allows the analysis of energy exchanges among the different types of oscillation. We obtain that the rate of energy exchanges is enhanced for chaotic orbits. Moreover, the highest rates for the coupling occur in the vicinity of the homoclinic tangle of the primary hyperbolic point embedded in a chaotic sea. The results demonstrate a clear relation between internal energy exchanges and the dynamics of coupled systems, being an efficient new way to distinguish regular from chaotic orbits.

© 2022 Elsevier B.V. All rights reserved.

A challenging problem of intrinsically coupled nonlinear Hamiltonian systems is the internal energy exchange among their components [1]. One example is the numerical investigation of energy exchanges among normal modes in the Fermi-Pasta-Ulam-Tsingou (FPUT) model of a nonlinear coupled oscillators chain, which presents a surprising energy concentration in some modes [2,3]. A reason for the observed results is the coexistence of regular and chaotic regions in the phase space of the coupled oscillators chain.

One of the difficulties related to the analysis of FPUT (and related) models is their large phase space dimension. In order to investigate with more depth the internal energy exchanges due to coupling between modes, we consider a paradigmatic low-dimensional system: the spring pendulum with two degrees of freedom [4]. This system exhibits an intrinsic nonlinear coupling, and we present numerical evidence that the rate of energy exchanges associated with the coupling is directly related to the regular or chaotic dynamics of the trajectories.

The spring pendulum, also known as elastic or extensible pendulum, is composed of a spring connected to a pivot on one end and to a suspended mass on the other end. The suspended mass can oscillate both harmonically, due to the spring elasticity, and pendularly, performing librations and rotations around the pivot due to the gravitational force. The combination of these two oscillation modes yields a complex and rich dynamics, with chaotic and resonant effects such as an order-chaos-order transition [5–8] and a parametric resonance [4,9–13] according to the total energy and the system parameters.

Besides having a complex dynamics, the spring pendulum is also investigated due to its similarities to other physical systems of great interest. Fermi already pointed out that the spring pendulum dynamics can be a mechanical analogy to the interaction of an atom with radiation [14]. Fermi also brought to the attention that the parametric resonance in the vibrations of the two degrees of freedom CO_2 molecule is similar to the spring pendulum parametric resonance [14–16]. Among other examples of systems described by equations analogous to those of the spring pendulum, we mention the orbits of celestial bodies [17–20], coupled waves in plasmas [21,22], interaction between light waves in a nonlinear dielectric [23], and several mechanical devices [24–27].

In a previous work, we introduced three analytical expressions for the energy associated with the spring, pendulum and coupled oscillations of a spring pendulum [28]. We applied these analytical expressions and verified that they accurately describe the energy components for periodic, quasi-periodic and chaotic trajectories. We then numerically computed phase space and time averages to

E-mail addresses: meirielenso@gmail.com (M. C. de Sousa), aschelin@gmail.com
(A.B. Schelin), albertus.marcus@gmail.com (F.A. Marcus), viana@fisica.ufpr.br
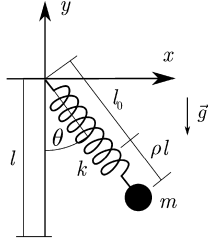(R. L. Viana), ibere@if.usp.br (I. L. Caldas).

Fig. 1. Spring pendulum diagram [Reprinted from M. C. de Sousa, F.A. Marcus, I. L. Caldas, R. L. Viana, Energy distribution in intrinsically coupled systems: the spring pendulum paradigm, Phys. A, Stat. Mech. Appl. 509 (2018) 1110-1119].

determine how the energy is distributed among the three components as a function of the total energy and a control parameter representing the ratio of the pendulum and spring frequencies.

In the present paper, we investigate the energy exchange rate (i.e. the power) for the previously identified energy components. We examine the phase space configuration for different values of total energy and control parameter, and we find that regular regions exhibit well defined power components, whereas chaotic regions display non-uniform values for the power components. Furthermore, the power associated with the coupling is generally higher for chaotic orbits than for regular ones. We also analyze the time dependence of the coupling power and verify that its maximum values in the Poincaré section follow the homoclinic tangle [29–31], which is composed of homoclinic intersections of the stable and unstable manifolds of the primary hyperbolic point immersed in a chaotic sea.

Such results show that the regular or chaotic dynamics observed for this nonlinear coupled system is determined by the rate of internal energy exchanges among its components, and that the coupling is closely related to the manifolds of hyperbolic points. In this sense, the approach we introduce may be a new and practical way to distinguish chaotic and regular orbits, as well as to access the manifolds of hyperbolic points with good precision.

The vertical spring pendulum presents a mass m connected to the free end of a spring with negligible mass, stiffness constant k and relaxed length l_0 in the absence of forces, as shown in Fig. 1. The other spring end is fixed at the origin of the Cartesian coordinate system $(x, y) = (0, 0)$. The spring pendulum moves in the vertical xy-plane and its stable equilibrium position is located at $x = 0$, $y = -l$, with $l = l_0 + mg/k$ and g the acceleration of gravity.

We write the Hamiltonian of this system in the dimensionless Cartesian coordinates $q_1 = x/l$ and $q_2 = (y + l)/l$, which are centered in the stable equilibrium position, and their associated momenta $p_1 = \dot{q}_1$ and $p_2 = \dot{q}_2$:

$$E_T = H = \frac{p_1^2 + p_2^2}{2} + f(q_2 - 1)$$
$$+ \frac{1}{2}(\sqrt{q_1^2 + (q_2 - 1)^2} + f - 1)^2, \tag{1}$$

where E_T is the dimensionless total energy, and $f = mg/(kl)$ is the square of the ratio between the pendulum and spring frequencies in the linear approximation, thus accounting for the physical characteristics of the spring pendulum.

As an example, we show in Fig. 2 the Poincaré section of the spring pendulum for $E_T = 0.3$ and $f = 0.25$, which displays a mixed dynamics typical of Hamiltonian systems, where islands of regular motion are embedded in the chaotic area. In fact, by increasing the total energy and/or control parameter f, the Poincaré sections of the spring pendulum reveal a peculiar sequence of order-chaos-order [5–8].

Following Ref. [28], we work with the dimensionless polar coordinates
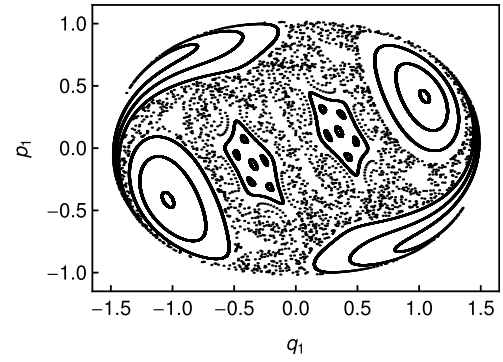

Fig. 2. Poincaré section $p_1 \times q_1$, with $q_2 = 0$ and $p_2 > 0$, for $E_T = 0.3$ and $f = 0.25$.

$$\rho = f - 1 + \sqrt{q_1^2 + (q_2 - 1)^2} \tag{2}$$

and

$$\tan\theta = \frac{q_1}{1 - q_2}, \tag{3}$$

where ρ represents the spring extension or compression from its relaxed length, and θ is the pendulum displacement from its stable equilibrium position.

The Hamiltonian in dimensionless polar coordinates is then given by [28]

$$E_T = H = \frac{1}{2}\left[p_\rho^2 + \frac{p_\theta^2}{(\rho + 1 - f)^2} \right]$$
$$+ \frac{\rho^2}{2} - (\rho + 1 - f)f\cos\theta. \tag{4}$$

In [28], we split the spring pendulum Hamiltonian into the spring, pendulum, and coupling energy components. The spring energy E_S characterizes a spring mass moving vertically under the action of gravity:

$$E_S = \frac{p_\rho^2 + \rho^2}{2} - (\rho + 1 - f)f. \tag{5}$$

The pendulum energy E_P describes the motion of a simple pendulum and is given by:

$$E_P = \frac{p_\theta^2}{2} - f\cos\theta. \tag{6}$$

The coupling energy E_C arises from the nonlinear coupling between the spring and pendulum oscillations. It is the only energy component that depends on both ρ and θ associated with the spring and pendulum respectively:

$$E_C = \frac{p_\theta^2}{2}\left[\frac{1}{(\rho + 1 - f)^2} - 1 \right]$$
$$- (\rho - f)f\cos\theta + (\rho + 1 - f)f. \tag{7}$$

From expressions (4)-(7), the total energy of the spring pendulum is given by

$$E_T = E_S + E_P + E_C. \tag{8}$$

These energy components are compatible with the spring and pendulum oscillations and account for their coupling. In Ref. [28], we applied the analytical expressions (5)-(7) to determine how the total energy is shared among the three components for individual trajectories. We verified that the energy components accurately describe the behavior of all kinds of trajectory: periodic, quasi-periodic and chaotic. By calculating phase space and time averages
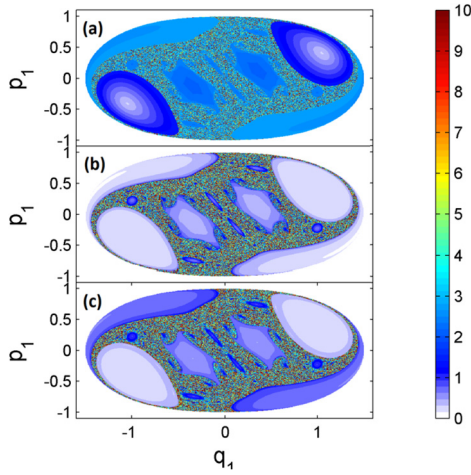
Fig. 3. (Color online.) Color scale showing the maximum power distribution in the section $p_1 \times q_1$ for $E_T = 0.3$ and $f = 0.25$: (a) spring power $P_{S,max}$, (b) pendular power $P_{P,max}$, and (c) coupling power $P_{C,max}$.

for a great number of trajectories, we also obtained the average energy distribution as a function of total energy and control parameter f. Once again, the average energy distribution is a good representation of the global dynamics in phase space for all possible values of E_T and f.

In this paper, we investigate how the energy is transferred among the three energy components as the system evolves in time. To do so, we consider the rate of energy exchange

$$P_i = \left| \frac{dE_i}{dt} \right|, \qquad (9)$$

where P_i corresponds to the power associated with each energy component (5)-(7), and the index i represents the type of oscillation: spring S, pendulum P, and coupled C.

Through the power terms (9), we investigate how the total energy is exchanged among the different types of oscillation that an orbit goes through during its time evolution. In Fig. 3, we consider the two-dimensional section p_1 vs q_1 (with $q_2 = 0$) of phase space, and plot in color scale the maximum power $P_{i,max}$ obtained for a long period of time, $t_f = 10^3$, in a grid of 600×600 initial conditions. By comparing Fig. 3 with the Poincaré section of Fig. 2, we notice that regular and chaotic regions are clearly distinguished from each other by their different values of maximum power. Regular trajectories have well defined values of maximum power, whereas initial conditions in the chaotic sea present non-uniform values of $P_{i,max}$.

The maximum power values of chaotic orbits are typically higher than those of regular orbits for all types of oscillation: spring, pendulum and coupled. It means that energy is exchanged at higher rates among the three types of oscillation when the orbit behaves chaotically. On the other hand, energy exchanges in regular trajectories occur at a much lower rate. Furthermore, we observe that the maximum pendulum power is almost null in the six main islands of regular behavior in Fig. 3. Thus, in these regions, energy is exchanged mostly between the spring and coupling energy components.

From now on, we will focus on the coupling power. To better understand the evolution of $P_{C,max}$ over time, we show in Fig. 4 the maximum value of coupling power integrated over different values of final time t_f. As time passes from panels (a) to (d), we observe the growth of the red filaments that correspond to the highest values of maximum coupling power ($2.5 \leq P_{C,max} \leq 3.0$).

By integrating the equations of motion backwards in time, we obtain another set of red filaments representing the highest values of maximum coupling power, as shown in Fig. 5. We combine
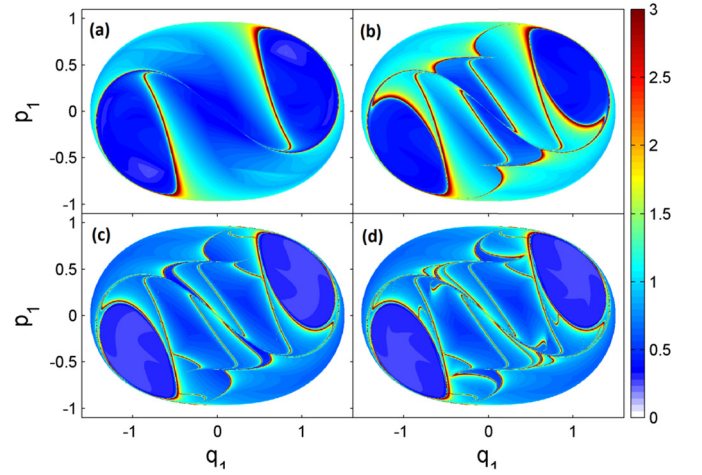

Fig. 4. (Color online.) Time evolution of the maximum coupling power for $t_i = 0$ and (a) $t_f = 10$, (b) $t_f = 20$, (c) $t_f = 30$ and (d) $t_f = 40$.
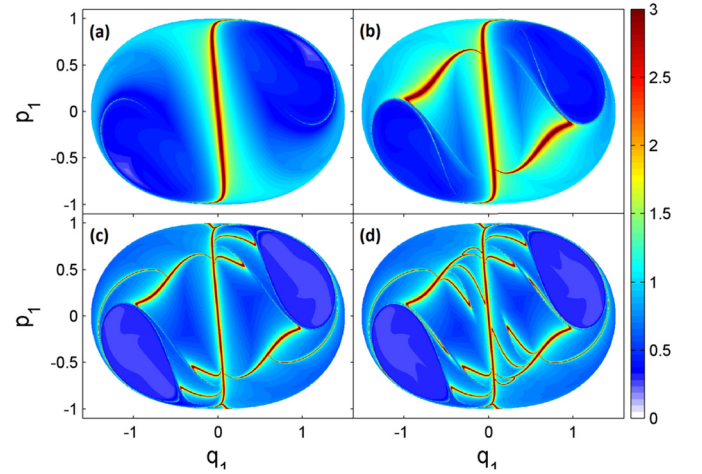

Fig. 5. (Color online.) Backward time evolution of the maximum coupling power for $t_i = 0$ and (a) $t_f = -10$, (b) $t_f = -20$, (c) $t_f = -30$ and (d) $t_f = -40$.

both Figs. 4 and 5 to exhibit in Fig. 6(a) the filaments with the highest values of maximum coupling power for $t_f = \pm 70$. In this figure, the red filaments were calculated by integrating the equations of motion forward in time, whereas the black filaments show the highest values of $P_{C,max}$ for the backward time evolution.

We also obtain the manifolds of the primary hyperbolic point $q_1 = p_1 = 0$, located in the chaotic region of Fig. 2, and compare them with the filaments of highest values of maximum coupling power. To calculate approximations for the invariant manifolds, we apply a standard numerical procedure [32]: we consider a disk of very small radius (10^{-6}) centered at the hyperbolic point $(q_1, p_1) = (0, 0)$, and containing a large number of initial conditions. Each initial condition belonging to the disk is numerically integrated from $t_i = 0$ to $t_f = 70$, generating a continuous flow. In Fig. 6(b), we plot in the section $p_1 \times q_1$ the intersections of this continuous flow with the plane $q_2 = 0$ whenever $p_2 > 0$. The plot (in red) turns out to be a spaghetti-like region following the unstable manifold that emanates from the periodic orbit with constant $(q_1, p_1) = (0, 0)$.

We also integrate the equations of motion backwards in time for the initial conditions within the tiny disk for $t_i = 0$ and $t_f = -70$. The plot in section $p_1 \times q_1$ [shown in black in Fig. 6(b)] is another spaghetti-like region now following the stable manifold of the primary hyperbolic point at $(q_1, p_1) = (0, 0)$. In Fig. 6(b), we
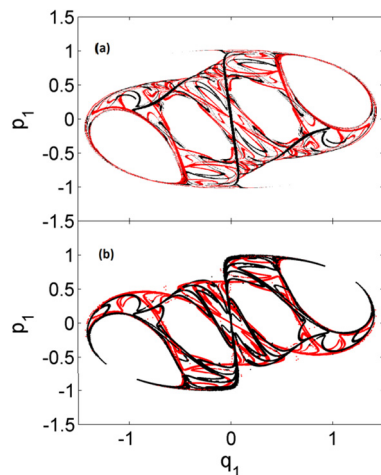
Fig. 6. (Color online.) (a) Filaments with highest values of maximum coupling power for $t_f = \pm 70$ obtained by integrating the equations of motion forward (red) and backwards (black) in time. (b) Unstable (red) and stable (black) manifolds of the primary hyperbolic point at $p_1 = q_1 = 0$.

display the superposition of the primary unstable (in red) and stable (in black) manifolds for the Poincaré section of Fig. 2.

Comparing Figs. 6(a) and 6(b), we identify the filaments of highest coupling power with the manifolds of the primary hyperbolic point $(q_1, p_1) = (0, 0)$. The filaments obtained for the forward time evolution correspond to the unstable manifold (both in red in Fig. 6), whereas the filaments for the backward time evolution represent the stable manifold (both in black).

The homoclinic tangle, which is formed by the intersections of the unstable and stable manifolds, is the source of the highest values of coupling power, i.e. it is responsible for the maximum energy exchange rate among the three different types of energy: spring, pendulum and coupling. Indeed, the homoclinic tangle influences all orbits in the chaotic area, which pass several times in its vicinity. In the same way, the homoclinic tangle leads to the higher energy exchange rates observed in the chaotic sea than in the regular regions of Fig. 3. It means that chaotic trajectories exchange energy at much higher rates between spring, pendulum and coupled oscillations, resulting in higher values of all power components $P_{i,max}$ as observed in Fig. 3.

In conclusion, we considered the spring pendulum, a paradigm of intrinsically coupled nonlinear systems, to investigate internal energy exchanges among the different kinds of oscillation it may present. We split the total energy among three energy components that accurately describe the spring, pendulum and coupled oscillations [28]. We then obtained analytical expressions for the energy exchange rate, i.e. the power, associated with each energy component.

We applied these expressions to determine the maximum values of the power components for a large number of trajectories. We observed that regular regions in phase space display well defined values of maximum power for all the components. On the other hand, chaotic areas can be distinguished by their non-uniform values of maximum power. Furthermore, chaotic trajectories generally present higher values of power than regular trajectories.

To determine the reason for the observed features, we analyzed the time evolution of the maximum coupling power in phase space, and identified the trajectories with the highest values of coupling power. We also computed the unstable and stable manifolds of the primary hyperbolic point of the system, and found that they correspond to the trajectories presenting the highest values of coupling power. It means that the coupling power is maximum along the primary manifolds and especially along the homoclinic

tangle formed by the intersections of the unstable and stable manifolds. Since chaotic trajectories pass frequently in the vicinity of the homoclinic tangle, the rate of internal energy exchange is much higher for these trajectories.

We confirmed for several values of total energy and control parameter that the maximum coupling power occurs along the manifolds of the primary hyperbolic point, and that all the power components are typically lower for regular trajectories than for chaotic ones. In a future work, we will investigate internal energy exchanges for other nonlinear coupled Hamiltonian systems in order to generalize the results presented in this paper, which may be a useful and efficient way to characterize chaotic orbits and to compute manifolds.

CRediT authorship contribution statement

M. C. de Sousa: Conceptualization, Data curation, Formal analysis, Funding acquisition, Investigation, Methodology, Validation, Writing – original draft, Writing – review & editing. **A.B. Schelin:** Data curation, Formal analysis, Investigation, Methodology, Validation, Visualization, Writing – original draft, Writing – review & editing. **F.A. Marcus:** Conceptualization, Data curation, Formal analysis, Investigation, Methodology, Validation, Writing – review & editing. **R. L. Viana:** Formal analysis, Funding acquisition, Investigation, Supervision, Validation, Writing – original draft, Writing – review & editing. **I. L. Caldas:** Conceptualization, Formal analysis, Funding acquisition, Investigation, Methodology, Project administration, Supervision, Validation, Writing – original draft, Writing – review & editing.

Declaration of competing interest

The authors declare that they have no known competing financial interests or personal relationships that could have appeared to influence the work reported in this paper.

Data availability

Data will be made available on request.

Acknowledgements

References

[1] J. Ford, The Fermi-Pasta-Ulam problem: paradox turns discovery, Phys. Rep. 213 (1992) 271.
[2] T. Dauxois, M. Peyrard, S. Ruffo, The Fermi-Pasta-Ulam 'numerical experiment': history and pedagogical perspectives, Eur. J. Phys. 26 (2005) S3.
[3] T. Dauxois, Fermi, Pasta, Ulam, and a mysterious lady, Phys. Today 61 (2008) 55.
[4] A. Vitt, G. Gorelik, Oscillations of an elastic pendulum as an example of the oscillations of two parametrically coupled linear systems, J. Tech. Phys. 3 (1933) 294.
[5] H.N. Núñez-Yépez, A.L. Salas-Brito, C.A. Vargas, L. Vicente, Onset of chaos in an extensible pendulum, Phys. Lett. A 145 (1990) 101.
[6] R. Cuerno, A.F. Rañada, J.J. Ruiz-Lorenzo, Deterministic chaos in the elastic pendulum: a simple laboratory for nonlinear dynamics, Am. J. Phys. 60 (1992) 73.
[7] R. Carretero-González, H.N. Núñez-Yépez, A.L. Salas-Brito, Regular and chaotic behaviour in an extensible pendulum, Eur. J. Phys. 15 (1994) 139.

[8] J.P. van der Weele, E. de Kleine, The order-chaos-order sequence in the spring pendulum, Physica A 228 (1996) 245.

[9] T.R. Kane, M.E. Kahn, On a class of two-degree-of-freedom oscillations, J. Appl. Mech. 35 (1968) 547.

[10] F.K. Tsel'man, On "pumping transfer of energy" between nonlinearly coupled oscillators in third-order resonance, J. Appl. Math. Mech. 34 (1970) 916.

[11] M.G. Rusbridge, Motion of the sprung pendulum, Am. J. Phys. 48 (1980) 146.

[12] E. Breitenberger, R.D. Mueller, The elastic pendulum: a nonlinear paradigm, J. Math. Phys. 22 (1981) 1196.

[13] H.M. Lai, On the recurrence phenomenon of a resonant spring pendulum, Am. J. Phys. 52 (1984) 219.

[14] E. Fermi, F. Rasetti, Über den Ramaneffekt des Steinsalzes, Z. Phys. 71 (1931) 689.

[15] G. Amat, M. Pimbert, On Fermi resonance in carbon dioxide, J. Mol. Spectrosc. 16 (1965) 278.

[16] B. Jacob, E.K.U. Gross, R.M. Dreizler, Solution of the Thomas-Fermi equation for triatomic systems, J. Phys. B 11 (1978) 3795.

[17] G. Contopoulos, Resonance cases and small divisors in a third integral of motion. I, Astron. J. 68 (1963) 763.

[18] G.-I. Hori, Theory of general perturbation with unspecified canonical variables, Publ. Astron. Soc. Jpn. 18 (1966) 287.

[19] R. Broucke, P.A. Baxa, Periodic solutions of a spring-pendulum system, Celest. Mech. 8 (1973) 261.

[20] D.L. Hitzl, The swinging spring - approximate analyses for low and very high energy, II, Celest. Mech. 12 (1975) 359.

[21] R.Z. Sagdeev, A.A. Galeev, Nonlinear Plasma Theory, Benjamin, New York, 1969, chap. I.

[22] W. Horton, Turbulent Transport in Magnetized Plasmas, World Scientific Publishing Co., Singapore, 2012.

[23] J.A. Armstrong, N. Bloembergen, J. Ducuing, P.S. Pershan, Interactions between light waves in a nonlinear dielectric, Phys. Rev. 127 (1962) 1918.

[24] P. Holmes, R.J. Full, D. Koditschek, J. Guckenheimer, The dynamics of legged locomotion: models, analyses, and challenges, SIAM Rev. 48 (2006) 207.

[25] N.D. Anh, H. Matsuhisa, L.D. Viet, M. Yasuda, Vibration control of an inverted pendulum type structure by passive mass-spring-pendulum dynamic vibration absorber, J. Sound Vib. 307 (2007) 187.

[26] D. Wang, J. Li, Q. Xie, Analytical model for dynamic tension in overhead power transmission lines subject to strong wind, Adv. Struct. Eng. 14 (2011) 445.

[27] S. Castillo-Rivera, M. Tomas-Rodriguez, Helicopter flap/lag energy exchange study, Nonlinear Dyn. 88 (2017) 2933.

[28] M.C. de Sousa, F.A. Marcus, I.L. Caldas, R.L. Viana, Energy distribution in intrinsically coupled systems: the spring pendulum paradigm, Phys. A, Stat. Mech. Appl. 509 (2018) 1110.

[29] A.M. Ozorio de Almeida, Hamiltonian Systems: Chaos and Quantization, Cambridge University Press, Cambridge, 1988.

[30] A.J. Lichtenberg, M.A. Lieberman, Regular and Chaotic Dynamics, 2nd edition, Springer, New York, 1992.

[31] J.D. Meiss, Symplectic maps, variational principles, and transport, Rev. Mod. Phys. 64 (1992) 795.

[32] H. Kantz, P. Grassberger, Repellers, semi-attractors, and long-lived chaotic transients, Phys. D: Nonlinear Phenom. 17 (1985) 75.